Low-Complexity SISO Equalization for AFDM with Time-Domain MRC Initialization

Chunjie Li
Sun Yat-sen University, Guangzhou, China
Pengcheng Laboratory, Shenzhen, China
lichj@pcl.ac.cn

Ke Zhang*
Pengcheng Laboratory
Shenzhen, China
zhangk@pcl.ac.cn

Ye Wang
Pengcheng Laboratory
Shenzhen, China
wangy02@pcl.ac.cn

Jian Jiao
Pengcheng Laboratory, Shenzhen, China
Harbin Institute of Technology, Shenzhen, China
jiaojian@hit.edu.cn

Xiao Ma
Sun Yat-sen University
Guangzhou, China
maxiao@mail.sysu.edu.cn

Qinyu Zhang
Pengcheng Laboratory, Shenzhen, China
Harbin Institute of Technology, Shenzhen, China
zqy@hit.edu.cn

***Abstract*—Affine frequency division multiplexing (AFDM) is a promising waveform for high-mobility communications over doubly selective channels. However, state-of-the-art iterative receivers typically achieve their strong detection performance by incorporating minimum mean square error (MMSE)-based equalization, whose repeated matrix operations impose substantial computational complexity. This paper proposes a low-complexity soft-input soft-output (SISO) equalization algorithm for AFDM. The proposed equalizer first exploits the sparsity of the time-domain channel matrix to perform maximum-ratio-combining (MRC) initialization, which provides reliable *a priori* estimates without matrix inversion. For the second stage, a discrete affine Fourier transform (DAFT)-domain SISO equalizer is then developed by formulating each symbol detection as a single-input multiple-output (SIMO) problem after interference cancellation. By embedding the proposed equalizer into an orthogonal approximate message passing (OAMP) receiver, we obtain a low-complexity OAMP (LC-OAMP) receiver, which enhances detection performance through soft information exchange with a low-density parity check (LDPC) decoder. Extensive simulation results demonstrate that the proposed LC-OAMP receiver achieves comparable error-rate performance to state-of-the-art schemes while significantly reducing computational complexity.**

***Index Terms*—Affine frequency division multiplexing (AFDM), soft-input soft-output (SISO) equalization, orthogonal approximate message passing (OAMP), doubly selective channels.**

I. Introduction

The sixth-generation (6G) wireless communication systems are expected to support unprecedented requirements in terms of data rate, connectivity, and mobility [1]. High-mobility scenarios, such as vehicular communications, high-speed trains, and low Earth orbit (LEO) satellites, pose significant challenges due to the time-varying nature of wireless channels. In such environments, the channel exhibits both delay spread and Doppler shift, leading to doubly dispersive channels that severely degrade the performance of traditional orthogonal frequency division multiplexing (OFDM) systems [2].

To address these challenges, affine frequency division multiplexing (AFDM) has emerged as a promising waveform for next-generation wireless communications [3]. Unlike OFDM, which relies on the Fourier transform and is optimal only for frequency selective channels, AFDM leverages the discrete affine Fourier transform (DAFT) to provide orthogonality in both delay and Doppler domains. This unique property enables AFDM to effectively combat the effects of doubly dispersive channels, making it particularly suitable for high-mobility scenarios [4].

To fully utilize the advantages of the AFDM system, low-complexity and high-performance equalization algorithms are essential. The conventional minimum mean square error (MMSE) equalizer can be applied to AFDM, but its cubic complexity is prohibitive. To reduce the complexity, the authors in [5] proposed a low-complexity MMSE equalizer based on the LDL factorization. The weighted maximum ratio combining (WMRC)-based decision feedback equalizer (DFE) was proposed in [2], where element-wise detection is performed iteratively. Different from the WMRC-DFE, a time-domain MRC equalization method proposed in [6] performs detection by exploiting the sparse lower-triangular structure of the time-domain channel matrix. Furthermore, message passing (MP) algorithms have also been investigated for AFDM detection [7]. Recently, the authors in [8] proposed a two-stage iterative MMSE equalizer with superior performance, but the computational complexity is high. In [9], the authors proposed a simplified expectation propagation equalizer, which employs diagonal reciprocity and single-pass MP for variance approximation and the incomplete LDL preconditioner to accelerate convergence.

While these pure equalization algorithms have shown promising results, performance can be further improved through iterative equalization and decoding architectures. In iterative equalization and decoding schemes, the equalizer and decoder exchange soft information iteratively, significantly enhancing detection reliability. Orthogonal approximate message passing (OAMP) combines AMP principles with orthogonal transformations to improve the convergence speed and accuracy of iterative receivers [10]. Its key idea is to

*Ke Zhang is the corresponding author.

979-8-3195-0167-7/26/$31.00 ©2026 IEEE

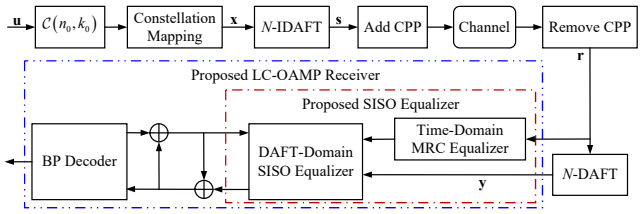


Fig. 1. Block diagram of the CPP-AFDM transceiver.

enforce orthogonality between the estimation errors of the linear estimator and the nonlinear estimator, which helps suppress error correlation during iteration and thereby enables more stable convergence [11]. OAMP has been successfully applied to AFDM with sparse code multiple access (SCMA) systems [12], where it demonstrates superior performance compared with the Turbo receiver [13]. However, the existing OAMP-assisted receiver relies on MMSE-based equalization, which involves matrix inversion and hence incurs cubic computational complexity. Therefore, AFDM receivers still face a challenging trade-off between detection performance and computational complexity.

In this paper, we propose a low-complexity SISO equalization algorithm for AFDM systems over doubly selective channels. By combining time-domain MRC-based initialization with DAFT-domain SISO equalization, the proposed equalizer avoids matrix inversion while maintaining reliable soft-output generation. Based on this equalizer, an LC-OAMP receiver with LDPC decoding is developed to further improve detection performance through soft information exchange. Simulation results demonstrate the effectiveness of the proposed LC-OAMP receiver.

II. System Model

In this section, we present the signal model for AFDM systems, including the AFDM modulation/demodulation process and the doubly selective channel model. Fig. 1 shows the transceiver diagram of the chirp-periodic prefix (CPP)-AFDM.

A. AFDM Modulation

Consider an AFDM system with N subcarriers. At the transmitter, the information bit vector $\mathbf{u} = (u_0, u_1, \ldots, u_{k_0-1})$ is first encoded using a linear block code $\mathcal{C}(n_0, k_0)$, where k_0 and n_0 represent the information bit length and coded bit length, respectively. The code rate is given by $R = k_0/n_0$. Let M denote the constellation size. Then each DAFT-domain symbol carries $\log_2 M$ bits, and the coded bit length satisfies $n_0 = N \log_2 M$. The coded bits are grouped into blocks of $\log_2 M$ bits and mapped to N complex symbols in the DAFT domain. Let $\mathbf{x} = (x_0, x_1, \ldots, x_{N-1})^T$ denote the DAFT-domain symbols, where each $x_m \in \mathcal{X}$ and $\mathcal{X}$ represents the constellation set. The time-domain signal is obtained by applying the inverse DAFT (IDAFT) as

$$s_n = \sum_{m=0}^{N-1} x_m \phi_n(m), \quad n = 0, \ldots, N-1, \tag{1}$$

where $\phi_n(m) = \frac{1}{\sqrt{N}} e^{j2\pi(c_1 n^2 + c_2 m^2 + \frac{nm}{N})}$, c_1 and c_2 are the chirp parameters. In matrix form, this can be expressed as $\mathbf{s} = \mathbf{\Lambda}_{c_1}^H \mathbf{F}_N^H \mathbf{\Lambda}_{c_2}^H \mathbf{x} = \mathbf{A}^H \mathbf{x}$, where $\mathbf{A} = \mathbf{\Lambda}_{c_2} \mathbf{F}_N \mathbf{\Lambda}_{c_1}$ is the DAFT matrix, $\mathbf{F}_N$ is the $N \times N$ DFT matrix, and $\mathbf{\Lambda}_c = \mathrm{diag}(e^{-j2\pi c n^2}, n = 0, 1, \ldots, N-1)$.

To combat multipath fading, a CPP of length L is appended to the time-domain signal. The CPP is defined as

$$s_n = s_{N+n} e^{-j2\pi c_1 (N^2 + 2Nn)}, n = -L, -L+1, \ldots, -1, \tag{2}$$

where L is chosen to be at least the maximum channel delay spread.

B. Doubly Selective Channel

We model the wireless channel as a doubly selective fading channel with P propagation paths. The time-varying channel impulse response at time n and delay l is given by

$$g_n(l) = \sum_{i=1}^{P} h_i e^{-j2\pi \nu_i n/N} \delta(l - l_i), \tag{3}$$

where h_i is the complex gain, $l_i \in [0, l_{\max}]$ is the path delay, $\nu_i = \alpha_i + \beta_i \in [-\nu_{\max}, \nu_{\max}]$ is the normalized Doppler shift with integer part $\alpha_i \in [-\alpha_{\max}, \alpha_{\max}]$ and fractional part $\beta_i \in (-1/2, 1/2]$, and $\alpha_{\max}$ is the maximum integer Doppler.

C. AFDM Demodulation

The received signal after transmission through the channel is expressed as

$$r_n = \sum_{l=0}^{l_{\max}} s_{n-l} g_n(l) + z_n, \quad n = 0, 1, \ldots, N-1, \tag{4}$$

where $z_n \sim \mathcal{CN}(0, N_0)$ denotes the additive white Gaussian noise (AWGN). After removing the CPP, the time-domain received signal can be written in matrix form as $\mathbf{r} = \mathbf{H}\mathbf{s} + \mathbf{z}$, where $\mathbf{H}$ is the time-domain channel matrix and an example is shown in Fig. 2(a). $\mathbf{H}$ can be expressed as

$$\mathbf{H} = \sum_{i=1}^{P} h_i \mathbf{\Gamma}_{\mathrm{CPP}_i} \mathbf{\Delta}_i \mathbf{\Pi}^{l_i}, \tag{5}$$

where $\mathbf{\Delta}_i = \mathrm{diag}(e^{-j2\pi \frac{\nu_i}{N} n}, n = 0, 1, \ldots, N-1)$, $\mathbf{\Pi}$ denotes the forward cyclic-shift matrix, i.e.,

$$\mathbf{\Pi} = \begin{bmatrix} 0 & \cdots & 0 & 1 \\ 1 & \cdots & 0 & 0 \\ \vdots & \ddots & \vdots & \vdots \\ 0 & \cdots & 1 & 0 \end{bmatrix}_{N \times N}, \tag{6}$$

and $\mathbf{\Gamma}_{\mathrm{CPP}_i}$ is a $N \times N$ diagonal matrix whose n-th diagonal entry is defined as

$$\Gamma_{\mathrm{CPP}_i}[n, n] = \begin{cases} e^{-j2\pi c_1 (N^2 - 2N(l_i - n))}, & n < l_i \\ 1, & n \geq l_i \end{cases}. \tag{7}$$

Applying the DAFT to the time-domain received signal yields

$$\mathbf{y} = \mathbf{A}\mathbf{r} = \mathbf{H}_{\mathrm{eff}} \mathbf{x} + \tilde{\mathbf{z}}, \tag{8}$$

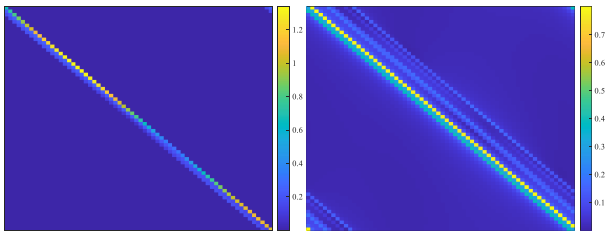


Fig. 2. Channel matrix characteristics in fractional Doppler scenarios: (a) Time-domain channel matrix, (b) DAFT-domain channel matrix.

where $\mathbf{H}_{\text{eff}} = \mathbf{A}\mathbf{H}\mathbf{A}^H$ is the effective channel matrix in the DAFT domain, and $\tilde{\mathbf{z}} = \mathbf{A}\mathbf{z}$ remains white Gaussian noise due to the unitarity of $\mathbf{A}$. The effective channel matrix can be decomposed into P path-specific components as

$$\mathbf{H}_{\text{eff}} = \sum_{i=1}^{P} h_i \mathbf{A}\mathbf{\Gamma}_{\text{CPP}_i}\mathbf{\Delta}_i\mathbf{\Pi}^{l_i}\mathbf{A}^H, \tag{9}$$

For integer Doppler shifts ($\beta_i = 0$), the DAFT-domain channel exhibits a sparse diagonal structure. However, fractional Doppler introduces power leakage, making $\mathbf{H}_{\text{eff}}$ less sparse, as shown in Fig. 2(b). To alleviate inter-path interference, we introduce a guard width ξ_ν and set $c_1 = \frac{2(\alpha_{\max}+\xi_\nu)+1}{2N}$.

III. LC-OAMP Receiver Design

This section presents the proposed LC-OAMP receiver for AFDM systems. We first introduce a time-domain MRC equalization method for initialization, which delivers *a priori* information to the subsequent iterative equalization and decoding process. Then, we describe the proposed DAFT-domain SISO equalization algorithm, followed by the OAMP framework for iterative equalization and decoding.

A. Time-Domain MRC Equalization

At the receiver, the time-domain MRC equalization leverages the sparse structure of the channel matrix to provide initial symbol estimates. Let $\tilde{P}$ indicate the number of resolvable multipath components in the time domain, satisfying $\tilde{P} \leq P$. Due to the sparse nature of the time-domain channel matrix $\mathbf{H}$, each column contains exactly $\tilde{P}$ non-zero entries among N total elements. We define $\mathcal{J}(n)$ as the set of row indices corresponding to the non-zero entries in the n-th column of $\mathbf{H}$, such that $|\mathcal{J}(n)| = \tilde{P}$.

We initialize the symbol estimates as $\hat{\mathbf{s}}^{(0)} = \mathbf{0}_{N\times 1}$, and set the residual error-plus-noise (REPN) vector to the received signal, i.e., $\Delta\mathbf{r}^{(0)} = \mathbf{r}$. In the t-th iteration, the transmitted symbols are estimated one by one. For the n-th symbol, we first collect the channel impaired terms as

$$\bar{s}_n^{(t)} = \sum_{d\in\mathcal{J}(n)} H^*[d,n]\Delta r_d^{(t-1)} + \bar{h}_n \hat{s}_n^{(t-1)}, \tag{10}$$

where $\bar{h}_n$ can be calculated as

$$\bar{h}_n = \sum_{d\in\mathcal{J}(n)} H^*[d,n]H[d,n]. \tag{11}$$

Algorithm 1 Time-Domain MRC Equalization

Input: $\mathbf{r}$, $\mathbf{H}$, γ, T_1, ϵ
Output: $\hat{\mathbf{s}}$

```
Initialize ŝ^(0) = 0_{N×1}, Δr^(0) = r
Calculate w according to Eq. (12)
for t = 1 to T_1 do
    for n = 0 to N − 1 do
        Calculate s̄_n^(t) according to Eq. (10)
        Calculate ŝ_n^(t) according to Eq. (13)
        for d ∈ J(n) do
            Update Δr_d^(t−1) according to Eq. (14)
        end for
    end for
    if ||ŝ^(t) − ŝ^(t−1)||_2 < ε then
        Break
    end if
    Δr^(t) = Δr^(t−1)
end for
return ŝ
```

The weighting vector $\mathbf{w} = (w_0, w_1, \ldots, w_{N-1})$ is computed element-wise, with each component given by

$$w_n = \bar{h}_n + \gamma^{-1}, \tag{12}$$

where γ is the signal-to-noise ratio (SNR). The symbol estimate is then obtained by

$$\hat{s}_n^{(t)} = \frac{\bar{s}_n^{(t)}}{w_n}. \tag{13}$$

Following the update of the n-th symbol, the values of $\Delta r_d^{(t-1)}, d \in \mathcal{J}(n)$ will be updated as

$$\Delta r_d^{(t-1)} = \Delta r_d^{(t-1)} - H[d,n]\left(\hat{s}_n^{(t)} - \hat{s}_n^{(t-1)}\right). \tag{14}$$

In the same way, we update the estimation results for the transmitted time-domain symbols sequentially in each iteration until the maximum number of iterations T_1 is reached or the difference of estimation results between two consecutive iterations has a 2-norm less than threshold ϵ, as summarized in Algorithm 1.

B. DAFT-Domain SISO Equalization

After the initial time-domain MRC equalization or after receiving feedback from the decoder during iterative equalization and decoding, the interference from other symbols can be effectively canceled. For the n-th symbol, we obtain a single-input multiple-output (SIMO) observation model as

$$\mathbf{y}_n^{\text{IC}} = \mathbf{h}_{\text{eff},n} x_n + \mathbf{w}_{\text{eff}}, \tag{15}$$

where $\mathbf{h}_{\text{eff},n}$ is the n-th column of the effective channel matrix $\mathbf{H}_{\text{eff}}$, and $\mathbf{w}_{\text{eff}} \sim \mathcal{CN}(\mathbf{0}, N_0\mathbf{I})$ represents the effective noise.

We assume that the transmitted symbols are independent and follow Gaussian *a priori* distributions, i.e.,

$$x_n \sim \mathcal{CN}(\mu_n^a, v_n^a), \tag{16}$$

where μ_n^a and v_n^a represent the *a priori* mean and variance of symbol x_n, respectively. These *a priori* statistics are provided by the decoder in the iterative receiver or the time-domain MRC equalizer.

For the SIMO model in Eq. (15), the *a posteriori* distribution of x_n is proportional to the product of the *a priori* distribution and the likelihood as

$$p(x_n \mid \mathbf{y}_n^{\text{IC}}) \propto \underbrace{\mathcal{CN}(x_n; \mu_n^a, v_n^a)}_{\textit{a priori}} \cdot \underbrace{\mathcal{CN}(\mathbf{y}_n^{\text{IC}}; \mathbf{h}_{\text{eff},n} x_n, N_0 \mathbf{I})}_{\text{likelihood}}. \tag{17}$$

Using the Gaussian product formula, the *a posteriori* distribution remains Gaussian. The *a posteriori* variance and mean are given by

$$v_n^p = \left(\frac{1}{v_n^a} + \frac{\tilde{h}_n}{N_0} \right)^{-1}, \tag{18}$$

$$\mu_n^p = v_n^p \left(\frac{\mu_n^a}{v_n^a} + \frac{\mathbf{h}_{\text{eff},n}^H \mathbf{y}_n^{\text{IC}}}{N_0} \right), \tag{19}$$

where $\tilde{h}_n = \mathbf{h}_{\text{eff},n}^H \mathbf{h}_{\text{eff},n}$.

In the t-th iteration, the interference-canceled signal $\mathbf{y}_n^{\text{IC},(t)}$ is not directly available. Instead, we compute it using the REPN $\Delta \mathbf{y}^{(t-1)} = \mathbf{y} - \mathbf{H}_{\text{eff}} \hat{\mathbf{x}}^{(t-1)}$, where $\hat{\mathbf{x}}^{(t-1)}$ is the symbol estimate from the $(t-1)$-th iteration. Note that we have

$$\mathbf{y}_n^{\text{IC},(t)} = \mathbf{y} - \sum_{m \neq n} \mathbf{h}_{\text{eff},m} \hat{x}_m^{(t-1)} = \Delta \mathbf{y}^{(t-1)} + \mathbf{h}_{\text{eff},n} \hat{x}_n^{(t-1)}. \tag{20}$$

Substituting (20) into (19) and using $\hat{x}_n^{(t-1)}$ from the $(t-1)$-th iteration, we obtain the update equation for the t-th iteration as

$$\hat{x}_n^{(t)} = v_n^p \left(\frac{\mu_n^a}{v_n^a} + \frac{\mathbf{h}_{\text{eff},n}^H \Delta \mathbf{y}^{(t-1)} + \tilde{h}_n \hat{x}_n^{(t-1)}}{N_0} \right). \tag{21}$$

After estimating one symbol, the values of $\Delta \mathbf{y}^{(t-1)}$ will be updated as

$$\Delta \mathbf{y}^{(t-1)} = \Delta \mathbf{y}^{(t-1)} - \mathbf{h}_{\text{eff},n} \left(\hat{x}_n^{(t)} - \hat{x}_n^{(t-1)} \right). \tag{22}$$

In the same way, we update the estimation results for the transmitted symbols sequentially in each iteration until the maximum number of iterations T_2 is reached or the difference of estimation results between two consecutive iterations has a 2-norm less than threshold ϵ.

Let $\hat{\mathbf{x}} = (\hat{x}_0, \hat{x}_1, \ldots, \hat{x}_{N-1})$ denote the final estimation results in the proposed DAFT-domain SISO equalization. After the iteration is stopped, the extrinsic mean and variance are computed as

$$v_n^e = \left(\frac{\kappa}{v_n^p} - \frac{1-\kappa}{v_n^a} \right)^{-1}, \tag{23}$$

$$\mu_n^e = v_n^e \left(\kappa \frac{\mu_n^p}{v_n^p} - (1-\kappa) \frac{\mu_n^a}{v_n^a} \right), \tag{24}$$

where $\kappa \in (0, 1]$ is a damping factor, and $\mu_n^p = \hat{x}_n$ denotes the *a posteriori* estimate obtained by the proposed DAFT-domain SISO equalization algorithm.

Algorithm 2 DAFT-Domain SISO Equalization

Input: $\mathbf{y}$, $\mathbf{H}_{\text{eff}}$, $\boldsymbol{\mu}^a$, $\boldsymbol{v}^a$, N_0, T_2, ϵ, κ
Output: $\boldsymbol{\mu}^e$, $\boldsymbol{v}^e$, $\mathbf{L}^e$

```
Initialize x̂^(0) = μ^a, Δy^(0) = y
Calculate h̃_n = h_{eff,n}^H h_{eff,n}, n = 0, ..., N − 1
Calculate v_n^p, n = 0, ..., N − 1 according to Eq. (18)
for t = 1 to T_2 do
    for n = 0 to N − 1 do
        Calculate x̂_n^(t) according to Eq. (21)
        Update Δy^(t−1) according to Eq. (22)
    end for
    if ||x̂^(t) − x̂^(t−1)||_2 < ε then
        Break
    end if
    Δy^(t) = Δy^(t−1)
end for
Calculate the extrinsic mean and variance according to Eqs. (23) and (24), respectively
Calculate the extrinsic LLRs according to Eqs. (25) and (26)
return μ^e, v^e, L^e
```

Based on the extrinsic mean and variance, the probability of x_n can be expressed as

$$P_E(x_n = x) \propto \exp\left(-\frac{|x - \mu_n^e|^2}{v_n^e} \right), \forall x \in \mathcal{X}. \tag{25}$$

The corresponding extrinsic log-likelihood ratios (LLRs) $\mathbf{L}^e = (L_0^e, L_1^e, \ldots, L_{n_0-1}^e)$ from the proposed DAFT-domain SISO equalization algorithm can be calculated as

$$L_{n \log_2 M + q}^e = \ln \frac{\sum_{x \in \mathcal{X}^{q,0}} P_E(x)}{\sum_{x \in \mathcal{X}^{q,1}} P_E(x)}, \quad n = 0, \ldots, N-1, \tag{26}$$

where $q = 0, \ldots, \log_2 M - 1$, $\mathcal{X}^{q,0}$ and $\mathcal{X}^{q,1}$ are subsets of $\mathcal{X}$ for which the q-th mapping bit is 0 and 1, respectively. The procedure of the proposed DAFT-domain SISO equalizer is summarized in Algorithm 2.

C. LC-OAMP Receiver Design for LDPC Codes

After performing the proposed SISO equalization, the extrinsic LLRs $\mathbf{L}^e$ are fed to the belief propagation (BP) decoder for LDPC codes. Then, the BP decoder outputs *a posteriori* LLRs $\mathbf{L}^p = (L_0^p, L_1^p, \ldots, L_{n_0-1}^p)$. To convert these LLRs into *a priori* information for the next iteration of the proposed DAFT-domain SISO equalizer, we first convert them into *a posteriori* probabilities as

$$P_D(x_n = x) \propto \prod_{q=0}^{\log_2 M - 1} \exp\left((1 - b_q) L_{n \log_2 M + q}^p \right), \tag{27}$$

where b_q denotes the q-th bit of symbol x.

The *a posteriori* mean and variance at the decoder output are given by

$$\mu_n^{\text{dec},p} = \sum_{x \in \mathcal{X}} x \cdot P_D(x_n = x), \tag{28}$$

Algorithm 3 LC-OAMP

Input: $\mathbf{r}$, $\mathbf{H}$, γ, T_1, $\mathbf{y}$, $\mathbf{H}_{\text{eff}}$, T_2, ϵ, κ, T, T_{BP}
Output: $\hat{\mathbf{u}}$

1: Obtain the estimation results $\hat{\mathbf{s}}$ according to Algorithm 1
2: Initialize $\boldsymbol{\mu}^a = \mathbf{A}\hat{\mathbf{s}}$, $\boldsymbol{v}^a = \mathbf{1}_{N\times 1}$, $\hat{\mathbf{u}}^{(0)} = \mathbf{0}_{n_0\times 1}$
3: **for** $t = 1$ **to** T **do**
4: Perform the proposed DAFT-domain SISO equalization according to Algorithm 2
5: Perform BP decoding and output the *a posteriori* LLRs $\mathbf{L}^p$ and hard-decision results $\hat{\mathbf{u}}^{(t)}$
6: Calculate the *a posteriori* probability according to Eq. (27)
7: Calculate the *a posteriori* mean and variance according to Eqs. (28) and (29), respectively
8: Calculate the extrinsic mean and variance according to Eqs. (30) and (31), respectively
9: **if** $\hat{\mathbf{u}}^{(t)} == \hat{\mathbf{u}}^{(t-1)}$ **then**
10: Break
11: **end if**
12: **end for**
13: **return** $\hat{\mathbf{u}}$

$$v_n^{\text{dec},p} = \sum_{x\in\mathcal{X}} |x|^2 \cdot P_D(x_n = x) - |\mu_n^{\text{dec},p}|^2. \tag{29}$$

Using the *a priori* mean and variance μ_n^a and v_n^a provided by the equalizer, the extrinsic mean and variance are obtained as

$$v_n^{\text{dec},e} = \left(\frac{1}{v_n^{\text{dec},p}} - \frac{1}{v_n^a}\right)^{-1}, \tag{30}$$

$$\mu_n^{\text{dec},e} = v_n^{\text{dec},e}\left(\frac{\mu_n^{\text{dec},p}}{v_n^{\text{dec},p}} - \frac{\mu_n^a}{v_n^a}\right), \tag{31}$$

which are fed back to the proposed DAFT-domain SISO equalizer as *a priori* information in the next iteration.

Let T denote the maximum number of iterations for the outer loop in the proposed LC-OAMP receiver. The iteration will be terminated when the estimation results converge or the maximum number of iterations is reached. The procedure of the proposed LC-OAMP receiver is summarized in Algorithm 3.

IV. Complexity and Convergence Analysis

This section focuses on the computational complexity and convergence behavior of the proposed LC-OAMP receiver. We first evaluate the computational complexity of the proposed LC-OAMP receiver by counting the required number of operations. Then, we study the convergence behavior of the proposed LC-OAMP receiver through the extrinsic information transfer (EXIT) chart analysis, which reveals the soft-information exchange between the proposed DAFT-domain SISO equalizer and the BP decoder.

A. Computational Complexity

In this subsection, the computational complexity of the proposed LC-OAMP receiver is evaluated in terms of real additions, binary additions, real multiplications, comparisons, and table look-ups. Note that we regard the operation of $\ln(\cdot)$ and $\exp(\cdot)$ as a table look-up. Besides, we regard 1 complex multiplication as 4 real multiplications and 2 real additions, and 1 complex addition as 2 real additions. Let T_a, $T_{1,a}$, $T_{2,a}$, and $T_{\text{BP},a}$ be the average number of iterations for the outer loop of the LC-OAMP receiver, the time-domain MRC equalizer, the DAFT-domain SISO equalizer, and the BP decoder, respectively.

We summarize the operations according to Algorithm 3. Step 1 of Algorithm 3 invokes Algorithm 1 only once. Next, we first summarize the operations in Algorithm 1. In Algorithm 1, step 2 is performed only once and requires $2\tilde{P}N$ real multiplications and $2\tilde{P}N$ real additions. Step 5 requires $4\tilde{P}+2$ real multiplications and $4\tilde{P}$ real additions. Step 6 requires 2 real multiplications. Steps 7 to 9 require $4\tilde{P}$ real multiplications and $6\tilde{P}$ real additions. Since there are N symbols to be estimated, the total operations from step 4 to 10 are $(8\tilde{P}+4)N$ real multiplications and $10\tilde{P}N$ real additions. Steps 11 to 13 require $2N+1$ real multiplications, $4N-1$ real additions, and 1 comparison. Consider the average iteration number $T_{1,a}$, the total operations of step 1 in Algorithm 3 are $2\tilde{P}N + ((8\tilde{P}+6)N+1)T_{1,a}$ real multiplications, $2\tilde{P}N + ((10\tilde{P}+4)N-1)T_{1,a}$ real additions, and $T_{1,a}$ comparisons.

Step 2 of Algorithm 3 calculates $\boldsymbol{\mu}^a = \mathbf{A}\hat{\mathbf{s}} = \boldsymbol{\Lambda}_{c_2}\mathbf{F}_N\boldsymbol{\Lambda}_{c_1}\hat{\mathbf{s}}$ requiring $2N\log_2 N + 8N$ real multiplications and $3N\log_2 N + 4N$ real additions. Step 4 executes Algorithm 2, the corresponding operations are summarized as follows. In Algorithm 2, step 2 requires $2N^2$ real multiplications and $2N^2 - N$ real additions. Step 3 requires $3N$ real multiplications and N real additions. Step 6 requires $4N+8$ real multiplications and $2N+4$ real additions. Step 7 requires $4N$ real multiplications and $2N+2$ real additions. Since there are N symbols to be estimated, the total operations from step 5 to 8 are $(8N+8)N$ real multiplications and $(4N+6)N$ real additions. Steps 9 to 11 require $2N+1$ real multiplications, $4N-1$ real additions, and 1 comparison. Consider the average iteration number $T_{2,a}$, the total operations from step 4 to 13 in Algorithm 2 are $((8N+10)N+1)T_{2,a}$ real multiplications, $((4N+10)N-1)T_{2,a}$ real additions, and $T_{2,a}$ comparisons. Step 14 requires $11N$ real multiplications and $3N+1$ real additions. Step 15 requires $3MN+n_0$ real multiplications and $3MN+(M-2)n_0$ real additions, and $MN+n_0$ table look-ups. In summary, the total operations of Algorithm 2 are $2N^2 + ((8N+10)N+1)T_{2,a} + 14N + 3MN + n_0$ real multiplications, $2N^2 + ((4N+10)N-1)T_{2,a} + 3N + 1 + 3MN + (M-2)n_0$ real additions, $T_{2,a}$ comparisons, and $MN+n_0$ table look-ups.

Step 5 of Algorithm 3 performs the BP decoding, and the total operations have been summarized in [14]. Step 6 requires $MN(\log_2 M - 1)$ real multiplications, $MN\log_2 M$ real additions, and $MN\log_2 M$ table look-ups. Step 7 requires $5MN+2N$ real multiplications and $4MN-N$ real additions. Step 8 requires $9N$ real multiplications and $3N$ real additions. Steps 9 to 11 require n_0 comparisons.

TABLE I
COMPUTATIONAL COMPLEXITY OF RECEIVERS

Operations	Conventional OAMP [12]	Turbo [13]	LC-OAMP
Binary additions	$m_0 n_0 T_{\text{BP},a} T_a$	$m_0 n_0 T_{\text{BP},a} T_a$	$m_0 n_0 T_{\text{BP},a} T_a$
Real additions	$(18N^3+16N^2+$ $6N+2n_0\bar{d}_v T_{\text{BP},a}+$ $MN\log_2 M+4MN)T_a$	$(18N^3+16N^2+$ $3N+2n_0\bar{d}_v T_{\text{BP},a}+$ $MN\log_2 M+4MN)T_a$	$2\tilde{P}N+((10\tilde{P}+4)N-1)T_{1,a}+3N\log_2 N+4N+$ $(2N^2+((4N+10)N-1)T_{2,a}+3N+1+3MN)T_a+$ $((M-2)n_0+2n_0\bar{d}_v T_{\text{BP},a}+MN\log_2 M+4MN+2N)T_a$
Real multiplications	$(20N^3+24N^2+20N+$ $m_0(2\bar{d}_c-1)T_{\text{BP},a}+5MN$ $+MN(\log_2 M-1))T_a$	$(20N^3+24N^2+11N+$ $m_0(2\bar{d}_c-1)T_{\text{BP},a}+5MN$ $+MN(\log_2 M-1))T_a$	$2\tilde{P}N+((8\tilde{P}+6)N+1)T_{1,a}+2N\log_2 N+8N+$ $(2N^2+((8N+10)N+1)T_{2,a}+14N+3MN+n_0)T_a+$ $(m_0(2\bar{d}_c-1)T_{\text{BP},a}+MN(\log_2 M-1)+5MN+11N)T_a$
Comparisons	$(n_0+(m_0+n_0)T_{\text{BP},a})T_a$	$(n_0+(m_0+n_0)T_{\text{BP},a})T_a$	$T_{1,a}+(T_{2,a}+n_0+(m_0+n_0)T_{\text{BP},a})T_a$
Table look-ups	$(MN+n_0+2m_0\bar{d}_c T_{\text{BP},a}$ $+MN\log_2 M)T_a$	$(MN+n_0+2m_0\bar{d}_c T_{\text{BP},a}$ $+MN\log_2 M)T_a$	$(MN+n_0+2m_0\bar{d}_c T_{\text{BP},a}+MN\log_2 M)T_a$

Consider the average iteration number T_a, the operations of the proposed LC-OAMP receiver are summarized in Table I. Furthermore, the operations of conventional OAMP receiver [12] and Turbo receiver [13] are also included. Note that the parity-check matrix has the size of $m_0 \times n_0$, $\bar{d}_v$ and $\bar{d}_c$ denote the average degrees of variable nodes and check nodes, respectively.

B. EXIT Chart Analysis

The extrinsic information transfer (EXIT) chart is a powerful tool for analyzing the convergence behavior of iterative equalization and decoding systems [15]. By tracking the exchange of extrinsic information between the equalizer and decoder, EXIT charts can predict whether the iterative process will converge without resorting to time-consuming bit error rate (BER) simulations. In the proposed LC-OAMP receiver, the outer loop consists of soft-information exchange between the proposed DAFT-domain SISO equalizer and the BP decoder, and is therefore characterized by two complementary transfer curves corresponding to these two modules.

Inspired by the empirical EXIT idea in [16], the two transfer curves are estimated by Monte Carlo simulations. Let I_E^a and I_E^e denote the *a priori* and extrinsic mutual information of the equalizer, respectively, and let I_D^a and I_D^e denote those of the decoder. As usual, the *a priori* LLRs are generated as

$$L_{E,n}^a = \frac{\sigma_a^2}{2} d_n + \sigma_a e_n, n = 0, 1, \ldots, n_0 - 1 \tag{32}$$

where $d_n \in \{+1, -1\}$, $e_n \sim \mathcal{N}(0,1)$, and σ_a is determined by [17]

$$I_E^a = 1 - \int_{-\infty}^{\infty} \frac{1}{\sqrt{2\pi\sigma_a^2}} \exp\left(-\frac{(\xi - \sigma_a^2/2)^2}{2\sigma_a^2}\right) \times \log_2(1+e^{-\xi})\, d\xi. \tag{33}$$

The generated *a priori* LLRs are mapped to *a priori* means and variances and then processed by the proposed DAFT-domain SISO equalizer together with the channel output. The output extrinsic LLRs of the equalizer are obtained according to Eq. (26). The extrinsic mutual information I_E^e can be calculated as

$$I_E^e = 1 - \mathbb{E}\left[\log_2\left(1 + e^{-dL_E^e}\right)\right], \tag{34}$$

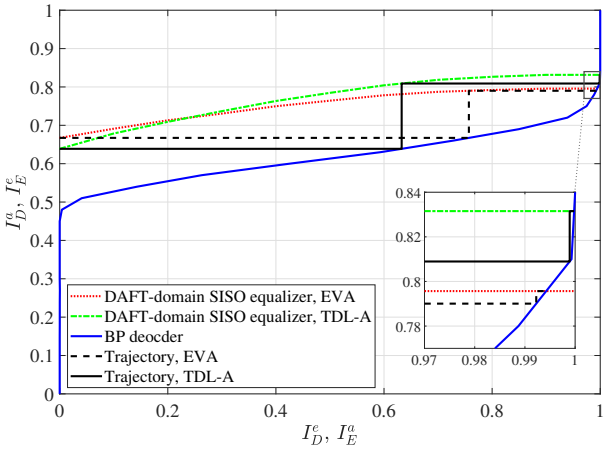


Fig. 3. The EXIT chart of the proposed LC-OAMP receiver with 5G LDPC code $\mathcal{C}(128, 64)$.

where $d \in \{+1, -1\}$ and L_E^e denote the transmitted bit and the extrinsic LLR, respectively. This expectation can be obtained by Monte Carlo simulation. Repeating this procedure for different values of I_E^a yields the complete equalizer EXIT curve. From Eq. (34), we can express I_E^e as a function of I_E^a and E_b/N_0 as

$$I_E^e = f_E(I_E^a, E_b/N_0). \tag{35}$$

The decoder EXIT curve is computed similarly. For a given I_D^a, we generate *a priori* LLRs according to Eq. (32) and feed them to the BP decoder. The extrinsic means and variances of the BP decoder are converted to the corresponding LLRs using Eqs. (25) and (26). The extrinsic mutual information I_D^e can also be calculated according to Eq. (34). Similarly, we can express I_D^e as a function of I_D^a as

$$I_D^e = f_D(I_D^a). \tag{36}$$

The convergence behavior of the iterative receiver can be analyzed by plotting both EXIT curves in the same figure, with I_D^e, I_E^a on the abscissa and I_D^a, I_E^e on the ordinate. Fig. 3 shows the EXIT chart of the proposed LC-OAMP receiver with 5G LDPC code $\mathcal{C}(128, 64)$, and the trajectories of iterative equalization and decoding are also presented. Note

TABLE II
SIMULATION PARAMETERS

Parameters	Values
Channel model	EVA [18], TDL-A [19]
Modulation	QPSK
LDPC code	5G LDPC codes $\mathcal{C}(128,64)$, $\mathcal{C}(128,96)$
Number of AFDM subcarriers	$N = 64$
Carrier frequency & Subcarrier spacing	$f_c = 4$GHz, $\Delta f = 15$kHz
Maximum normalized Doppler shift	$\nu_{\max} = 1$
Chirp parameters	$c_1 = \frac{2(\alpha_{\max}+\xi_\nu)+1}{2N}\|_{\xi_\nu=1}$ $c_2 = \frac{1}{N^2}$

that E_b/N_0 is set to 6 dB for the Extended Vehicular A (EVA) [18] and Tapped Delay Line-A (TDL-A) [19] channels. The other parameters can be found in Section V. From Fig. 3, the decoding trajectories for both channels exhibit typical staircase-like exchanges between the equalizer and decoder transfer curves. Moreover, the EXIT chart provides useful insights into the convergence region of the proposed LC-OAMP receiver and the average number of iterations required for convergence. As observed from the number of staircase steps in Fig. 3, three iterations are sufficient for the proposed LC-OAMP receiver to approach its expected performance.

V. SIMULATION RESULTS

In this section, simulation results are presented to evaluate the error performance and computational complexity of the proposed LC-OAMP receiver. We consider two channel models, namely the EVA [18] and TDL-A [19]. In all simulations, the parameters are summarized in Table II. The Doppler shift for each path is generated using Jakes' formula, i.e., $\nu_p = \nu_{\max}\cos\theta_p$, where $\theta_p \sim \mathcal{U}[-\pi,\pi]$. For comparison, conventional OAMP [12] and Turbo [13] receivers are also included. Unless otherwise specified, the maximum outer-loop iteration number is set to $T = 6$, while the maximum iteration numbers of the time-domain MRC equalizer, the DAFT-domain SISO equalizer, and the BP decoder are set to $T_1 = 6$, $T_2 = 6$, and $T_{\mathrm{BP}} = 30$, respectively. In addition, the damping factor is set to $\kappa = 0.5$ and the stopping threshold is chosen as $\epsilon = 10^{-4}$. The performance is evaluated in terms of BER and average number of operations per information bit. Two 5G LDPC codes, i.e., $\mathcal{C}(128,64)$ and $\mathcal{C}(128,96)$, are considered to verify the effectiveness of the proposed LC-OAMP receiver under different code rates.

Fig. 4 illustrates the BER performance of various receivers with the 5G LDPC code $\mathcal{C}(128,64)$. It can be observed that the proposed LC-OAMP receiver achieves similar performance to the existing receivers under the EVA channel. Under the TDL-A channel, the proposed LC-OAMP receiver exhibits comparable performance to conventional OAMP, and both outperform the Turbo receiver. For instance, at a BER of 10^{-5}, the proposed LC-OAMP receiver provides approximately 0.5 dB gain over the Turbo receiver. Fig. 5 presents the BER performance with the higher-rate 5G LDPC code $\mathcal{C}(128,96)$.

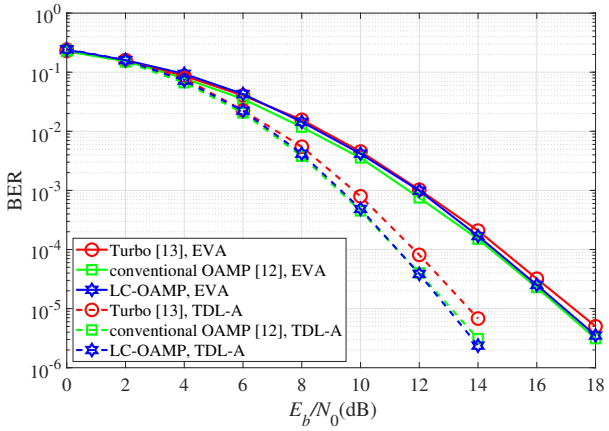


Fig. 4. BER performance comparisons of different receivers with 5G LDPC code $\mathcal{C}(128,64)$.

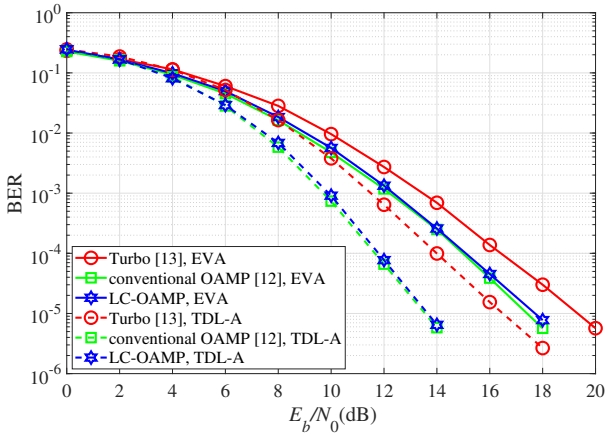


Fig. 5. BER performance comparisons of different receivers with 5G LDPC code $\mathcal{C}(128,96)$.

It can be observed that the proposed LC-OAMP receiver achieves a performance very close to that of the conventional OAMP receiver, while both significantly outperform the Turbo receiver. More specifically, at a BER of 10^{-5}, the proposed LC-OAMP receiver provides gains of approximately 1.5 dB and 2.5 dB over the Turbo receiver under the EVA and TDL-A channels, respectively.

Fig. 6 compares the computational complexity of different receivers for the 5G LDPC code $\mathcal{C}(128,64)$. It can be seen that the conventional OAMP receiver and the Turbo receiver both incur relatively high computational complexity, mainly because their iterative equalization stages involve matrix-related operations with high computational cost. By contrast, the proposed LC-OAMP receiver achieves the lowest computational complexity among all compared receivers. The main reason is that the proposed LC-OAMP receiver avoids matrix inversion and replaces the MMSE-based equalization with the proposed SISO equalizer. Therefore, the complexity reduction is achieved at the algorithmic level rather than through a simple reduction in the number of iterations. A similar trend can be observed in Fig. 7 for the 5G LDPC code $\mathcal{C}(128,96)$. The

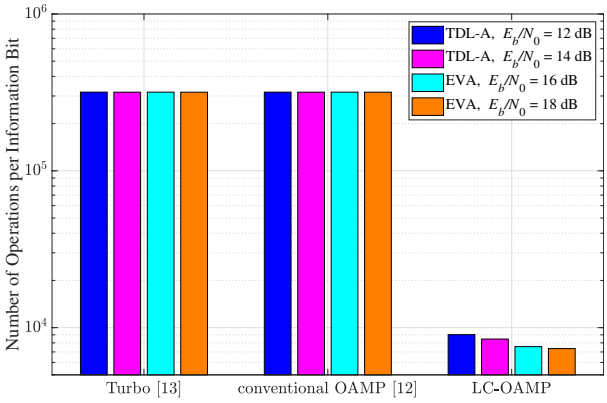


Fig. 6. Complexity comparisons of different receivers with 5G LDPC code $\mathcal{C}(128, 64)$.

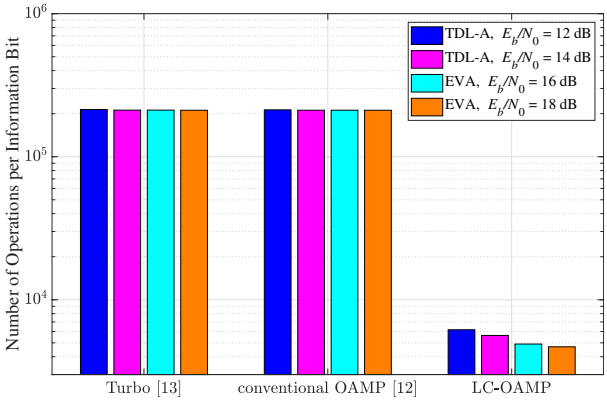


Fig. 7. Complexity comparisons of different receivers with 5G LDPC code $\mathcal{C}(128, 96)$.

proposed LC-OAMP receiver consistently maintains the lowest computational complexity, whereas the conventional OAMP and Turbo receivers still incur significantly higher complexity. In particular, compared with the conventional OAMP receiver, the proposed LC-OAMP receiver reduces the computational complexity by approximately 97%, while still preserving a BER performance close to that of the conventional OAMP receiver. This clearly demonstrates that the proposed LC-OAMP receiver achieves a more favorable trade-off between the performance and computational complexity.

VI. Conclusion

In this paper, we proposed a low-complexity SISO equalization algorithm for AFDM systems over doubly selective channels. The proposed equalizer combines time-domain MRC-based initialization with DAFT-domain SISO equalization, thereby avoiding matrix inversion while maintaining reliable soft-output generation. By incorporating the proposed equalizer into an OAMP receiver, we developed an LC-OAMP receiver that enables efficient equalization and decoding with substantially reduced computational complexity. Simulation results verified that the proposed LC-OAMP receiver attains performance close to the conventional OAMP receiver with much lower complexity.

Acknowledgment

This work was supported by the National Natural Sciences Foundation of China (NSFC) under Grant No. 62501331, and in part by the Major Key Project of PCL under Grant PCL2024A01.

References

[1] C.-X. Wang et al., "On the road to 6G: Visions, requirements, key technologies and testbeds," *IEEE Commun. Surveys Tuts.*, vol. 25, no. 2, pp. 905–974, 2nd Quart., 2023.

[2] A. Bemani, N. Ksairi, and M. Kountouris, "Affine frequency division multiplexing for next generation wireless communications," *IEEE Trans. Wireless Commun.*, vol. 22, no. 11, pp. 8214–8229, Nov. 2023.

[3] A. Bemani, N. Ksairi, and M. Kountouris, "AFDM: A full diversity next generation waveform for high mobility communications," in *Proc. IEEE Int. Conf. Commun. Workshops (ICC Workshops)*, Jun. 2021, pp. 1–6.

[4] Q. Li, J. Li, M. Wen, X. Dang, H. Arslan, and N. Al-Dhahir, "Affine frequency division multiplexing for 6G networks: Fundamentals, opportunities, and challenges," *IEEE Netw.*, vol. 40, no. 1, pp. 88–97, Jan. 2026.

[5] A. Bemani, N. Ksairi, and M. Kountouris, "Low complexity equalization for AFDM in doubly dispersive channels," in *Proc. IEEE Int. Conf. Acoust., Speech Signal Process. (ICASSP)*, May 2022, pp. 5273–5277.

[6] Q. Yi, Z. Sui, and Z. Liu, "Error rate analysis and low-complexity receiver design for zero-padded AFDM," 2025, *arXiv:2510.14507*.

[7] L. Wu, S. Luo, D. Song, F. Yang, and R. Lin, "A message passing detection based affine frequency division multiplexing communication system," *Digit. Signal Process.*, vol. 153, Art. no. 104633, Oct. 2024.

[8] C. Shen, J. Yuan, and J. Tong, "Time-domain zero-padding (TZP) AFDM with two-stage iterative MMSE detection," *IEEE Trans. Wireless Commun.*, vol. 25, pp. 6255–6269, 2026.

[9] C.-W. Chen, Y.-M. Lee, S.-C. Wang, C.-H. Kuo, and A.-Y. Wu, "PCG-based expectation propagation detector with message-passing initialization and approximated variance for fractional Doppler AFDM," *IEEE Wireless Commun. Lett.*, vol. 15, pp. 345–349, 2026.

[10] J. Ma, L. Liu, X. Yuan, and L. Ping, "On orthogonal AMP in coded linear vector systems," *IEEE Trans. Wireless Commun.*, vol. 18, no. 12, pp. 5658–5672, Dec. 2019.

[11] L. Liu, S. Liang, and L. Ping, "On capacity optimality of OAMP: Beyond IID sensing matrices and Gaussian signaling," *IEEE Trans. Commun.*, vol. 72, no. 5, pp. 2519–2535, May 2024.

[12] Q. Luo et al., "AFDM-SCMA: A promising waveform for massive connectivity over high mobility channels," *IEEE Trans. Wireless Commun.*, vol. 23, no. 10, pp. 14421–14436, Oct. 2024.

[13] Z. Liu and L.-L. Yang, "Sparse or dense: A comparative study of code-domain NOMA systems," *IEEE Trans. Wireless Commun.*, vol. 20, no. 8, pp. 4768–4780, Aug. 2021.

[14] C. Li, K. Zhang, J. Jiao, Y. Wang, X. Ma, and Q. Zhang, "Ultra-reliable receiver for asynchronous SCMA in satellite-terrestrial communication," *IEEE Trans. Commun.*, vol. 74, pp. 7074–7089, 2026.

[15] Y. Ge, Q. Deng, P. C. Ching, and Z. Ding, "OTFS signaling for uplink NOMA of heterogeneous mobility users," *IEEE Trans. Commun.*, vol. 69, no. 5, pp. 3147–3161, May 2021.

[16] J. Xu, X. Ma, K. Niu, and C. Dong, "SIC-based UAMP detection for MIMO-OTFS under fractional delay-Doppler channel," *IEEE Wireless Commun. Lett.*, vol. 13, no. 6, pp. 1745–1749, Jun. 2024.

[17] S. Ten Brink, "Convergence behavior of iteratively decoded parallel concatenated codes," *IEEE Trans. Commun.*, vol. 49, no. 10, pp. 1727–1737, Oct. 2001.

[18] *User Equipment (UE) radio transmission and reception (Release 19)*, document TS 36.101, 3GPP, 2026.

[19] *Study on channel model for frequencies from 0.5 to 100 GHz (Release 19)*, document TR 38.901, 3GPP, 2026.